Anyonic interferometry and protected memories in atomic spin lattices

LIANG JIANG[1]*, GAVIN K. BRENNEN[2,3], ALEXEY V. GORSHKOV[1], KLEMENS HAMMERER[2,3], MOHAMMAD HAFEZI[1], EUGENE DEMLER[1], MIKHAIL D. LUKIN[1] AND PETER ZOLLER[2,3]

[1]Physics Department, Harvard University, Cambridge, Massachusetts 02138, USA
[2]Institute for Theoretical Physics, University of Innsbruck, 6020 Innsbruck, Austria
[3]Institute for Quantum Optics and Quantum Information of the Austrian Academy of Science, 6020 Innsbruck, Austria
*e-mail: jiang@physics.harvard.edu

Published online: 20 April 2008; doi:10.1038/nphys943

Strongly correlated quantum systems can exhibit exotic behaviour called topological order which is characterized by non-local correlations that depend on the system topology. Such systems can exhibit remarkable phenomena such as quasiparticles with anyonic statistics and have been proposed as candidates for naturally error-free quantum computation. However, anyons have never been observed in nature directly. Here, we describe how to unambiguously detect and characterize such states in recently proposed spin–lattice realizations using ultracold atoms or molecules trapped in an optical lattice. We propose an experimentally feasible technique to access non-local degrees of freedom by carrying out global operations on trapped spins mediated by an optical cavity mode. We show how to reliably read and write topologically protected quantum memory using an atomic or photonic qubit. Furthermore, our technique can be used to probe statistics and dynamics of anyonic excitations.

By definition, topologically ordered states[1] cannot be distinguished by local observables, that is, there is no local order parameter. They can arise as ground states of certain hamiltonians that have topological degeneracy and that provide robustness against noise and quasilocal perturbations. These properties of such systems are attractive for quantum memories. However, the local indistinguishability makes measuring and manipulating the topological states difficult because they are only coupled by global operations. One way to access this information is to measure properties of the low-lying particle-like excitations. In two dimensions, the quasiparticles act like punctures in a surface that can have anyonic statistics and their topological properties are probed by braiding different particle types around each other. The existence of anyons also implies a topological degeneracy[2]. Quantum Hall fluids at certain filling fractions are believed to have topological order and there is a vigorous experimental effort to verify anyonic statistics in these systems[3]. A standard approach is to carry out some kind of interferometry that looks for non-trivial action on the fusion-state space on braiding. This is manifested as the evolution of a non-trivial statistical phase in the abelian case, or a change in the amplitude of the participating states in the non-abelian case. Some experimental evidence consistent with observation of abelian anyonic statistics in a $\nu = 2/5$-filled Quantum Hall state has been reported[4], but an unambiguous detection of anyons is still considered an open issue[5].

Spin–lattice hamiltonians can also exhibit topological order[6] and such hamiltonians can be built with atoms[7] or molecules[8] trapped in an optical lattice. A significant advantage of using atomic systems is that the microscopic physics is well known and there are established techniques for coherent control and measurement. Suggestions have been made for how to design anyonic interferometers in these systems by using local spin operations to guide excitation along braiding paths[9–11].

Here, we present a new approach that directly measures topological degeneracy and anyonic statistics using global operations. The technique involves coupling between a probe qubit (single ancilla spin qubit or optical mode) and topologically ordered atomic spins in an optical lattice. A many-body interaction between spins is mediated by coupling to a common bosonic mode of the radiation field using techniques of cavity quantum electrodynamics[12–15] or, alternatively, using a common phonon mode in ion traps[16]. Our approach avoids localizing and guiding excitations while enabling the measurement of the statistical phase associated with arbitrary braiding paths.

We also note that recent experiments have demonstrated braiding operations on small networks of non-interacting qubits encoded in photon polarization[17,18], which generates a simulation of anyonic interferometry[19]. However, because the background hamiltonian vanishes in such systems, they are not protected from noise and the particle interpretation of the 'excitations' is ambiguous. In contrast, the technique developed here enables us to probe directly dynamic evolution of anyonic quasiparticles within the parent hamiltonian. In addition, our mechanism can be used to carry out reading and writing of qubits initially encoded in light or atoms into topological memory, which may be useful for offline storage during a computation and for applications in long-distance quantum communication[20,21].

ATOMIC AND MOLECULAR SPIN LATTICES IN OPTICAL CAVITIES

We focus on physical systems in which a two-dimensional (2D) optical lattice (Fig. 1) is placed within a high-finesse optical cavity

© 2008 Nature Publishing Group

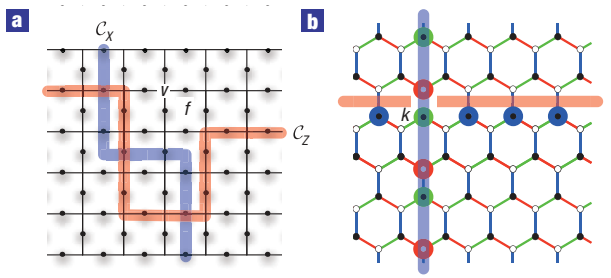

Figure 1 Generators for the encoded qubits. a, A planar code that encodes one logical qubit in the ground states. There is a spin-1/2 particle (filled circle) for each edge of the lattice. The interactions of the local hamiltonian $H_{\rm surf}$ are along edges that bound a face f, and edges that meet at a vertex v. The strings $\mathcal{C}_{X,Z}$ indicate paths of products of $\sigma^{x,z}$ operators that are logical operators on the code. **b**, A nearest-neighbour local hamiltonian $H_{\rm hcb}$ on the honeycomb lattice, with a spin-1/2 particle for each lattice site. The green (red, blue) edges represent interactions of type $\sigma^x\sigma^x(\sigma^y\sigma^y, \sigma^z\sigma^z)$ with coupling strength $J_x(J_y, J_z)$. In the limit that the interactions along the blue links are much stronger than those along the other links, the ground subspace has a gapped $\mathbb{Z}_2$ topological phase[6]. Physical σ^x (σ^y, σ^z) spin operations as part of the strings $\mathcal{C}_{X,Z}$ are indicated by bold green (red, blue) circles around the spins. We may implement the vertical string operation in two steps: first apply σ^x rotations to the spins with green circles and then apply σ^y rotations to the spins with red circles. Each step can be implemented with selective addressing[26,27]. At qubit k, the string crossing, the operation is $\sigma^x_k\sigma^z_k$.

as shown in Fig. 2a. To be specific, we consider the 2D square lattice hamiltonian introduced by Kitaev[22] where each edge of the lattice represents a spin-1/2 particle (Fig. 1a). Each vertex v or each face f is associated with an operator $H_v = \prod_{j\in{\rm star}(v)}\sigma^x_j$ or $H_f = \prod_{j\in\partial f}\sigma^z_j$. These operators collide on an even number of edges and hence mutually commute. We seek to encode in the $+1$ coeigenspace of these local stabilizers by choosing the so-called surface-code hamiltonian:

$$H_{\rm surf} = -J\sum_v H_v - J'\sum_f H_f.$$

($J, J' > 0$.) The ground states of $H_{\rm surf}$ have a degeneracy $\dim\mathcal{H}_{\rm gr} = 2^{2g+h}$ where g is the genus of the surface and h is the number of holes[23]. Designing lattices with genus $g > 0$, such as the surface of a torus, is challenging, but it is possible to create several holes ($h > 0$) in a planar lattice by, for instance, deactivating regions of the lattice with focused far-detuned lasers. Alternatively, the planar code with specific boundary as shown in Fig. 1a provides a ground-state degeneracy of 2. The logical states are coupled by the operators $\tilde{Z} = \prod_{j\in\mathcal{C}_Z}\sigma^z_j$ and $\tilde{X} = \prod_{j\in\mathcal{C}_X}\sigma^x_j$ where the configurations $\mathcal{C}_Z(\mathcal{C}_X)$ are strings on the lattice (dual lattice) as shown in Fig. 1a.

There are several experimental proposals to implement the spin–lattice hamiltonians with topological order. For example, Kitaev's honeycomb-lattice hamiltonian $H_{\rm hcb}$ (Fig. 1b)[6] can be designed in optical lattices with ultracold atoms using controlled spin-exchange interactions[7,24], or with molecules using microwave-induced dipole–dipole interactions[8]. With an appropriate choice of coupling parameters[6], the honeycomb-lattice hamiltonian has a gapped abelian phase with a low-energy effective hamiltonian locally equivalent to $H_{\rm surf}$. In the following, we will assume the system interacts through $H_{\rm surf}$, but our results are also applicable to other spin–lattice hamiltonians.

Now, we consider how to implement the global operations for the spin–lattice system. In particular, we are interested in a specific type of global operation: products of Pauli operators on a set of spins whose corresponding edges in the lattice form a connected string. Such global operators are called string operators. For example, the generators for the encoded qubits ($\tilde{Z}$ and $\tilde{X}$) are string operators (Fig. 1a). All string operators are equivalent to $S^z_{\mathcal{C}} = \prod_{j\in\mathcal{C}}\sigma^z_j$ up to local single-spin rotations, where $\mathcal{C}$ is the set of selected spins. In particular, $S^x_{\mathcal{C}} = \prod_{j\in\mathcal{C}}\sigma^x_j = (\prod_j H_j)S^z_{\mathcal{C}}(\prod_j H_j)$, where $(\prod_j H_j)$ is the global Hadamard rotation on all memory spins with H_j for the jth spin. Thus, we can use two global Hadamard rotations to convert $S^z_{\mathcal{C}}$ to $S^x_{\mathcal{C}}$.

In our set-up, the topological memory consists of a spin lattice of trapped atoms or molecules inside an optical cavity as shown in Fig. 2a. The off-resonant interaction between the common cavity mode and selected spins is described by the quantum non-demolition (QND) hamiltonian[25]:

$$H = \chi a^\dagger a\sum_{j\in\mathcal{C}}\sigma^z_j. \qquad (1)$$

Here, we assume that the cavity mode has a large detuning Δ from a spin-dependent optical transition as shown in Fig. 2b. The coupling strength is $\chi = g^2/2\Delta$, where g is the single-photon Rabi frequency for the cavity mode. The QND hamiltonian preserves the photon number $n_a = a^\dagger a$ of the cavity mode. In addition, the cavity mode also interacts with an ancilla spin, which will be used to probe anyonic statistics associated with quasiparticles.

Similar to the previous schemes[9,11] to measure anyonic statistics, we assume selective addressing of spins in the lattice so that we can carry out single-spin rotations. The key new ingredient, however, is that we use the common cavity mode to mediate global string operators. We assume that a string of selected atoms can be coupled to the common cavity mode simultaneously, using a control laser beam with an appropriately shaped intensity profile[26,27] as described in the Methods section. In this way, we avoid problems involving maintaining adiabaticity and localization while braiding quasiparticles. And most importantly, we are able to achieve controlled-string operations ($\Lambda[S^{x,z}_{\mathcal{C}}]$) for an arbitrary string $\mathcal{C}$.

The idea of controlled-string operations can be illustrated by considering a situation when the cavity mode is first prepared in some superposition of zero- and one-photon states. Within this subspace, the evolution of the QND hamiltonian for interaction time $\tau = \pi/2\chi$ yields

$$U = \exp[-iH\tau] = \left[(-i)^{N_{\mathcal{C}}}\prod_{j\in\mathcal{C}}\sigma^z_j\right]^{n_a}$$
$$= \begin{cases}\mathbf{I} & \text{for } n_a = 0\\ (-i)^{N_{\mathcal{C}}}\prod_{j\in\mathcal{C}}\sigma^z_j & \text{for } n_a = 1,\end{cases} \qquad (2)$$

where $N_{\mathcal{C}}$ is the number of elements in $\mathcal{C}$, and the second equality uses the identity $\exp[-i(\pi/2)\sigma^z_j] = -i\sigma^z_j$. This unitary evolution will apply the string operator $S^z_{\mathcal{C}}$ to the topological memory, conditioned on one cavity photon. With such controlled-string operations, we can conveniently access the topological memory, and build anyonic interferometry to probe braiding statistics and dynamics of quasiparticles.

In practice, however, it is actually easier to control the ancilla spin rather than to directly manipulate the photon number state. Therefore, in the following, we will present two approaches to controlled-string operations between the ancilla spin and the topological memory.

© 2008 Nature Publishing Group

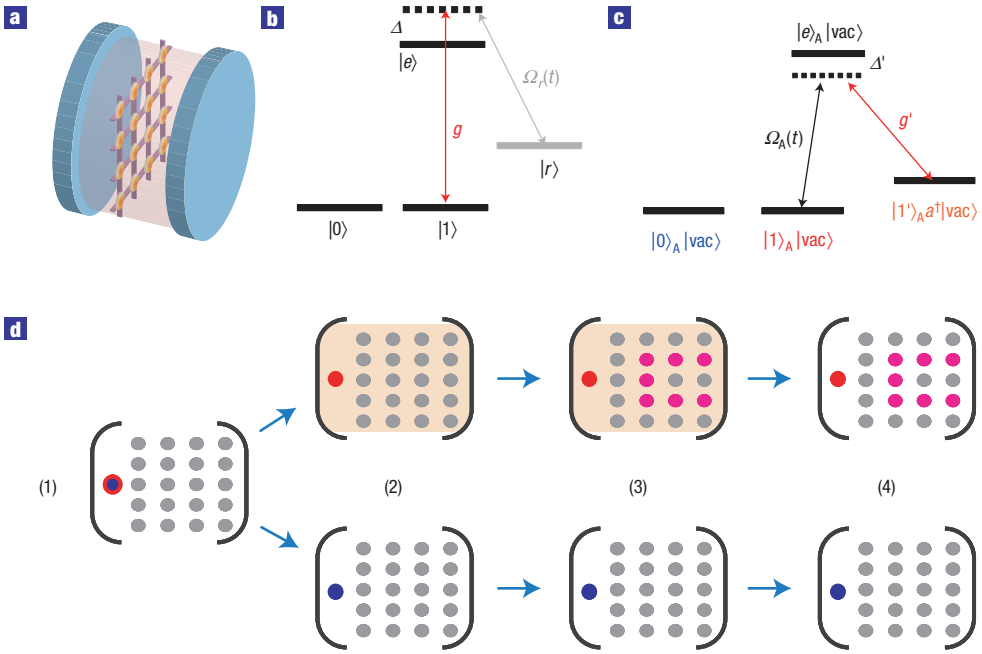

Figure 2 Cavity-assisted controlled-string operation based on the single-photon approach. a, Inside a cavity, an optical lattice carries spins for topological memory, with individual spin addressability[26,27]. **b**, The energy levels of a selected memory spin ($|0\rangle$ and $|1\rangle$) interacting dispersively with the cavity mode, which implements the QND hamiltonian of equation (1). The coupling coefficient is $\chi = g^2/\Delta$, with single-photon Rabi frequency g and detuning Δ from the excited state $|e\rangle$. A control laser with Rabi frequency $\Omega_r(t)$ couples to the metastable state $|r\rangle$, and it is in two-photon resonance with the cavity mode. **c**, The energy levels of the ancilla spin (different from memory spins) and the cavity mode for the single-photon approach. A different control laser with Rabi frequency $\Omega_A(t)$ connects the states $|1\rangle_A \otimes |\text{vac}\rangle$ and $|1'\rangle_A \otimes a^\dagger|\text{vac}\rangle$, and enables coherent creation and absorption of a cavity photon conditioned on the ancilla spin. **d**, Schematic diagram of the procedure for the implementation of the single-photon approach for controlled-string operations. (1) Initialize the ancilla spin (the left highlighted spin) in a superposition state $\alpha|0\rangle_A + \beta|1\rangle_A$ (blue for $|0\rangle_A$ and red for $|1\rangle_A$), with no photon in the cavity and state $|\psi\rangle_S$ for the topological memory. (2) Coherently create a cavity photon (orange shading) for ancilla spin state $|1\rangle_A$ (upper branch); no photon is created for ancilla spin state $|0\rangle_A$ (lower branch). (3) Switch on the interaction between the cavity photon and the selected spins. If there is a cavity photon (orange shading), a non-trivial evolution S^z_C (pink circles) is implemented. (4) Turn off the interaction and coherently absorb the cavity photon into the ancilla spin. Finally, the state $\alpha|0\rangle_A \otimes |\psi\rangle_S + \beta|1\rangle_A \otimes S^z_C|\psi\rangle_S$ is prepared.

CONTROLLED-STRING OPERATIONS

The key operation of the single-photon approach is the evolution of the QND interaction described by equation (2). In addition, the cavity mode interacts with a single ancilla spin using spectroscopically resolvable energy levels as shown in Fig. 2c. Starting with no photon in the cavity mode $|\text{vac}\rangle$ and the ancilla spin in state $\alpha|0\rangle_A + \beta|1\rangle_A$, we can coherently couple the number state of the cavity mode with the state of the ancilla spin by adiabatically increasing the Rabi frequency $\Omega_A(t)$ of the control laser until it is much larger than the single-photon Rabi frequency g'. The intermediate state is then $\alpha|0\rangle_A \otimes |\text{vac}\rangle - \beta|1'\rangle_A \otimes a^\dagger|\text{vac}\rangle$, having the photon number fully correlated with the ancilla spin. Applying the QND interaction with the intermediate state realizes the desired controlled-string operation conditioned on the state of the ancilla spin. Finally, we can reverse the state mapping by adiabatically decreasing the Rabi frequency, which coherently annihilates the photon of the cavity mode and restores the ancilla spin to its logical subspace spanned by $\{|0\rangle_A, |1\rangle_A\}$. Following the procedure summarized in Fig. 2d, we can achieve the controlled-string operation:

$$\Lambda\left[S^z_C\right] = |1\rangle_A\langle 1| \otimes S^z_C + |0\rangle_A\langle 0| \otimes \mathbf{I}. \qquad (3)$$

The second approach to controlled-string operations is based on the idea of geometric phase gates[28]. Here, the bosonic field of the cavity mode starts in a coherent state, rather than a superposition of zero- and one-photon states. If our transformation restores the bosonic field to the initial coherent state, the entire system will accumulate a quantum phase (geometric phase), which is twice the area enclosed by the trajectory in phase space of the bosonic field. We activate the geometric phase gate using an ancilla spin which experiences the QND interaction with the cavity mode that can be selectively turned on and off[26,27]. As shown in Fig. 3 and detailed in the Methods section: if the ancilla spin is in state $|0\rangle_A$, the enclosed area vanishes; if the ancilla spin is in state $|1\rangle_A$, the enclosed area has a different sign depending on whether the topological memory is in $+1$ or -1 subspace associated with the string operator S^z_C, yielding again equation (3).

Various imperfections such as the addressing error, photon loss and deviation of the QND interaction can degrade the controlled-string operation. The influence from these imperfections can be effectively minimized—a deep optical lattice should be applied to suppress the addressing error $N_C\varepsilon_{\text{address}}$, a cavity with high Purcell factor P can be used to reduce the photon loss[29,30] and quantum control techniques may be introduced to correct the deviation of the QND interaction to arbitrarily high order[31,32]. In addition, if we use Kitaev's honeycomb-lattice model[6] (Fig. 1b) to implement the toric-code hamiltonian, there will be an extra error associated with the string operation, $N_C\varepsilon_{\text{hcb}} \approx N_C(J_x^2 + J_y^2)/4J_z^2$ (where J_x, J_y and J_z are the coupling parameters between neighbouring sites defined in Fig. 1b), owing to the effective leakage

© 2008 Nature Publishing Group

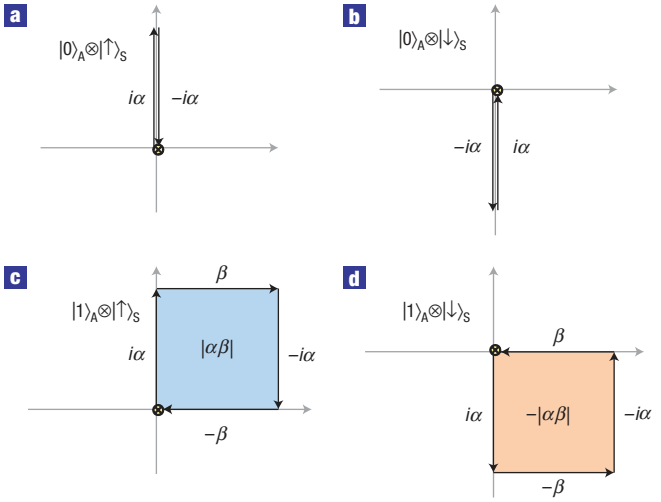

Figure 3 Phase accumulation for the geometric phase gate approach (equation (7)). We use $|\uparrow\rangle_S$ and $|\downarrow\rangle_S$ to represent $+1$ and -1 subspaces of memory spins associated with the string operator S^z_C, respectively. **a**,**b**, When the ancilla spin is in the $|0\rangle_A$ state, the enclosed area vanishes. **c**,**d**, When the ancilla spin is in the $|1\rangle_A$ state, for the subspace $|\uparrow\rangle_S$ the enclosed area is $|\alpha\beta|$ (**c**), and for the subspace $|\downarrow\rangle_S$ the enclosed area is $-|\alpha\beta|$ (**d**). The quantum phase accumulated is twice the area enclosed.

from the low-energy manifold[33]. As discussed in the Methods section and Supplementary Information, the error probability for controlled-string operation is approximately

$$\varepsilon_{\text{string}}(N_C) \approx \lambda\sqrt{N_C/P} + N_C(\varepsilon_{\text{address}} + \varepsilon_{\text{hcb}}), \qquad (4)$$

where the prefactor $\lambda = 2\pi$ (and $4\pi^2$) is for the single-photon (and geometric phase gate) approach.

ACCESSING TOPOLOGICAL QUANTUM MEMORY

Controlled-string operations provide an interface between the probe qubit which features easy access and efficient manipulation, and the topological memory which provides good storage. To store quantum states, we require two operations: the SWAP_{in} gate which swaps the state of a probe qubit A to memory M initialized in $|\tilde{0}\rangle_M$ and the SWAP_{out} which swaps back to a probe qubit prepared in $|0\rangle_A$.

$$\text{SWAP}_{\text{in}} = H_A \cdot \Lambda[\tilde{Z}] \cdot H_A \cdot \Lambda[\tilde{X}],$$

$$\text{SWAP}_{\text{out}} = \Lambda[\tilde{X}] \cdot H_A \cdot \Lambda[\tilde{Z}] \cdot H_A,$$

where H_A is the Hadamard gate acting on the probe qubit and $\Lambda[\tilde{S}]$ represents a controlled-string operation. In addition, universal rotations of the encoded qubit (generally, arbitrary unitaries generated by string operators) over the topological memory can be implemented either by teleportation of quantum gates or by direct geometric phase gates (see Supplementary Information for details). We remark that the ancilla spin can also be entangled with another ancilla spin from a different cavity, and therefore our topological memories can be used for quantum networks[34–37].

To compare the topological memory and unprotected single-spin memory, we introduce the decoherence rate q for the unprotected spin due to low-frequency noise. The topological memory can significantly reduce the decoherence rate to $q \times (\delta h/J)^N$, where $\delta h \ll J$ is the magnitude of the noise perturbation on individual spins and N is the length of the minimal string associated with the generators for encoded qubits[22]. Meanwhile, errors associated with four controlled-string operations $4\varepsilon_{\text{string}}(N)$ should be taken into account. Therefore, in terms of total error probability, the topological memory outperforms the single-spin memory for storage time $t > 4\varepsilon_{\text{string}}(N)/q$ (see Supplementary Information for details).

ANYONIC INTERFEROMETRY

Now, we describe how to use controlled-string operations to extract the statistical phase acquired when braiding abelian anyons. The definition of anyonic statistics usually relies on the adiabatic transport of quasiparticles around each other[38], with the required condition of adiabaticity to keep the system in the same manifold of excited states and prevent exciting extra degrees of freedom. Note that this procedure relies explicitly on the existence of the hamiltonian. This is fundamentally different from anyonic simulation approaches[17–19] not using a topological hamiltonian, which only probe the non-trivial commutation relations of spin operators and initially entangled quantum states. However, anyonic statistics is a property of quasiparticles associated with the hamiltonian and not just with some specially prepared initial state.

For our spin–lattice system with H_{surf}, there are two types of anyon[22]: (1) z-particles on the vertices and (2) x-particles on the faces of the lattice (Fig. 4a,b). These anyons are created in pairs (of the same type) by string operators: $|\psi^z(l)\rangle = S^z_l|\xi\rangle$ and $|\psi^x(l)\rangle = S^x_{l'}|\xi\rangle$, where $|\xi\rangle$ is some ground state of the spins, and $S^z_l = \prod_{j\in l}\sigma^z_j$ and $S^x_{l'} = \prod_{j\in l'}\sigma^x_j$ are string operators associated with string l on the lattice and string l' on the dual lattice, respectively (Fig. 4). In our approach, string operators can be used to effectively move quasiparticles quickly along the string trajectory but without exciting other quasiparticles. For example, effective motion of quasiparticles with/without braiding is shown in Fig. 4a,b. This evolution is described by

$$S^x_{l'_4} U_{t_3} S^z_{l_3} U_{t_2} S^x_{l'_2} U_{t_1} S^z_{l_1} |\Psi_{\text{initial}}\rangle = e^{i\theta_{\text{tot}}} |\Psi_{\text{initial}}\rangle, \qquad (5)$$

where we introduce time delays, represented by unitary evolution U_t, between string operations. The goal of these delays is to check that the system stays in the manifold with a fixed number of quasiparticles where time delays lead to only a trivial dynamical phase. On the other hand, if the string operator were to create some complicated intermediate states, time delays would lead to complete decoherence. The total phase $e^{i\theta_{\text{tot}}}$ includes both the dynamical contribution $e^{i\eta} = e^{i4J(t_1+t_2)+i4J'(t_2+t_3)}$ and the statistical contribution $e^{i\theta} = -1$ (or $+1$) in the presence (or absence) of braiding. Therefore, we can unambiguously measure the statistical phase if we can measure $e^{i\theta_{\text{tot}}}$ for both cases.

The following interference experiment can be used to measure the phase $e^{i\theta_{\text{tot}}}$. First, we prepare the probe qubit in a superposition state $(|0\rangle + |1\rangle)/\sqrt{2}$. We then use controlled-string operations to achieve interference of the following two possible evolutions: if the probe qubit is in state $|0\rangle$, no operation is applied to the memory spins; if the probe qubit is in state $|1\rangle$, the operation $S^x_{l'_4} U_{t_3} S^z_{l_3} U_{t_2} S^x_{l'_2} U_{t_1} S^z_{l_1}$ is applied to the topological memory, which picks up the extra phase $e^{i\theta_{\text{tot}}}$ we want to measure. After the controlled-string operations, the probe qubit will be in state $(|0\rangle + e^{i\theta_{\text{tot}}}|1\rangle)/\sqrt{2}$. Finally, we project the probe qubit to the basis of $|\xi_\pm\rangle \equiv (|0\rangle \pm e^{i\phi}|1\rangle)/\sqrt{2}$ with $\phi \in [0, 2\pi)$, and measure the operator $\sigma_\phi \equiv |\xi_+\rangle\langle\xi_+| - |\xi_-\rangle\langle\xi_-|$. The measurement of $\langle\sigma_\phi\rangle$ versus ϕ should have fringes with perfect contrast and a maximum shifted by $\phi = \theta_{\text{tot}}$. In fact, this scheme can be used to measure abelian

© 2008 Nature Publishing Group

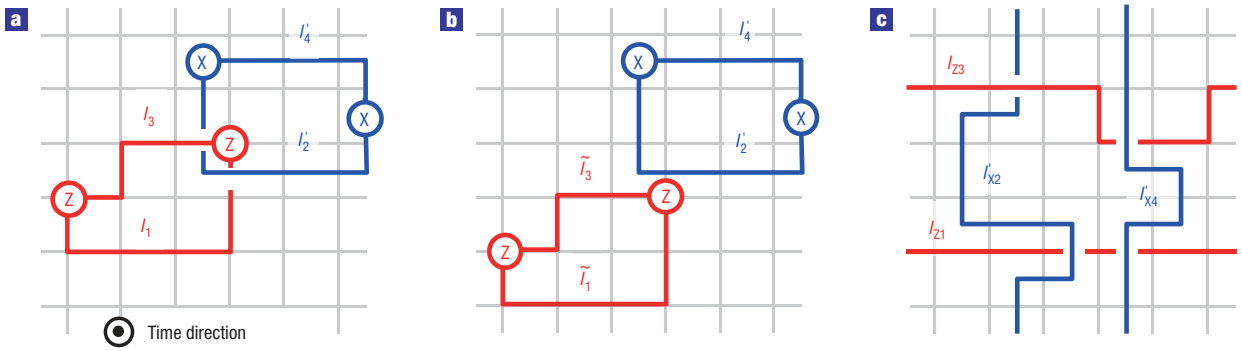

Figure 4 Braiding operations. a,**b**, We can move *x*-particles and *z*-particles in tangled/untangled loops using string operators to implement operations with/without braiding of anyons. **c**, We can also apply generators for the encoded qubits to achieve the braiding operation. The braiding statistics of anyons should be invariant under non-crossing deformations of the loops[39].

statistics for an arbitrary finite cyclic group as described in the Methods section.

It is crucial to verify that the outcome of the anyonic interferometry is invariant under repeated experiments with deformed string operators[39] (Fig. 4). For example, the two ground states of the 2D compass model[40] are coupled by perpendicular global X and Z string operators and the phase measured using the interferometry scheme above would also yield a phase -1 due to the anti-commutation relations at the crossing spin. Yet the ground states are not topologically ordered because deformed string operators do not preserve the ground subspace. As our anyonic interferometry can test all possible braiding operations, we can unambiguously verify the topological property of anyons.

Various imperfections will degrade the signature of anyonic statistics. The string operators may have errors that excite unwanted anyons, and the topological memory may not fully restore to the ground state after braiding. In addition, the topological memory may have anyons from imperfect initialization. If these anyons are enclosed by the braiding loops, they will affect the phase factor associated with braiding. However, neither of these imperfections will prevent us from probing anyonic statistics, because they only reduce the contrast of the anyonic interferometry without shifting the fringes of $\langle\sigma_\phi\rangle$. We may even distinguish the two types of imperfection from the contrast. The reduction of the contrast is proportional to the length of the loops for errors from string operators, whereas it is proportional to the area enclosed by the loops for errors from imperfect initialization (see discussion in the Methods section).

PROBING AND CONTROL OF ANYONIC DYNAMICS

Our anyonic interferometry provides a tool to study the dynamics of anyons. First, consider repeating the protocol (equation (5)) for anyonic interferometry with the time delays $\{t_j\}_{j=1,2,3}$ between the four controlled-string operations. Processes of anyonic creation, propagation, braiding and annihilation will induce a time dependence of the final-state wavefunction in a general expression: $|\Psi_{\text{final}}\rangle = \alpha(\{t_j\})|\Psi_{\text{initial}}\rangle + \beta(\{t_j\})|\Psi_\perp(\{t_j\})\rangle$, where $\langle\Psi_{\text{initial}}|\Psi_\perp(\{t_j\})\rangle = 0$. As the reduced density matrix of the probe qubit is $\rho = 1/2\begin{pmatrix} 1 & \alpha(\{t_j\}) \\ \alpha^*(\{t_j\}) & 1 \end{pmatrix}$, we can measure the complex coefficient $\alpha(\{t_j\})$ using quantum-state tomography[41] of the probe qubit.

Probing anyonic statistics can be regarded as special cases, with $\alpha = e^{i(\theta+\eta)}$ or $e^{i\eta}$, and $\beta = 0$. Although the anyons are immobile for the surface-code hamiltonian, the mobility of quasiparticles may change when we include local perturbations, because the excited states with anyons are highly degenerate and any small perturbation to the hamiltonian can dramatically change the eigenwavefunctions. Consider for example a specific diffusion model for anyons induced by the local perturbation

$$H_{\text{pert}} = \sum_{\alpha\in\{x,y,z\}} \sum_{e\in\text{all spins}} h_e^\alpha \sigma_e^\alpha, \qquad (6)$$

where the $h_e^{x,z}$ field components cause diffusion of $x(z)$-particles and the h_e^y field component causes diffusion of fermionic particles (pairs of neighbouring x-particles and z-particles) (see Supplementary Information for details). The nature of the perturbation (for example, time independent or changing with time) determines diffusion dynamics of anyons, which can be observed from the coefficient $\alpha(\{t_j\})$ using our anyonic interferometry.

In addition, we can even control the diffusion dynamics of anyons. We introduce the effective time-reversal operations $U_\pi^z \equiv \prod_{e\in\text{all spins}} \sigma_e^z$ and $U_\pi^x \equiv \prod_{e\in\text{all spins}} \sigma_e^x$, which anti-commute with $h_e^x\sigma_e^x$ and $h_e^z\sigma_e^z$ terms of H_{pert}, respectively. The combination of these operations (for example, $U_\pi^{z\,\tau/4}\cdots\cdots U_\pi^{x\,\tau/4}\cdots\cdots U_\pi^{z\,\tau/4}\cdots\cdots U_\pi^{x\,\tau/4}\cdots\cdots$) is analogous to spin-echo pulses in NMR[42], which can effectively reverse anyonic diffusion caused by static perturbations and consequently extend the fringe contrast of anyonic interferometry to longer time delays, as shown in Fig. 5. In essence, by applying these global operations, we can localize the anyons without any trapping potential (see Supplementary Information for details). Note that the anyonic interferometry is closely related to the Ramsey experiments in atomic physics, which can now be carried out with anyonic quasiparticles.

OUTLOOK

Controlled-string operations can be applied to other lattice hamiltonians as well[43,44], which may provide robust quantum memory with their degenerate ground states. For example, subsystem codes[43] can be constructed out of 2D and 3D nearest-neighbour spin-1/2 interactions that are realizable with atomic systems[7,8]. Our approach can be adapted to carry out the logical operations generated by strings or planes of Pauli operators in the 2D and 3D subsystem codes, respectively. In addition, the ability to measure global operators on a spin lattice provides a means to probe other properties of topological phases. For example, a class of topologically ordered spin states known as string net

© 2008 Nature Publishing Group

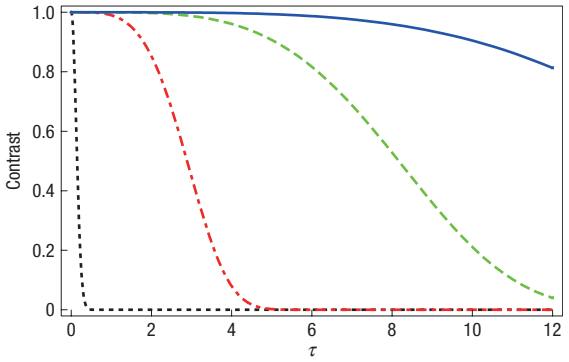

Figure 5 Fringe contrast of anyonic interferometry as a function of time (in units of $\langle (h_e^x)^2 \rangle^{-1/2}$) for anyonic diffusion. The fringe contrast quickly reduces owing to anyonic diffusion (black dotted line). However, we can extend the fringe contrast to longer times by applying one (red dotted–dashed line), four (green dashed line) or ten (blue solid line) pairs of time-reversal operations of U_π^z within the time interval τ. For clarity, we consider only the diffusion of two intermediate x-particles induced by the perturbation $h_e^x \sigma_e^x$ from equation (6). We assume that the controlled-string operations are ideal and the random field h_e^x is a gaussian random process with correlation time $\tau_c = 10$ (see Supplementary Information for details).

states[45], which includes the ground states of $H_{\rm surf}$, have the property that they are invariant under large closed-loop operations. In the present case, these operators are $X_{\rm loop}(Z_{\rm loop}) = \prod_{j \in C^{\rm closed}_{X,Z}} \sigma^{x,z}$ which have expectation value 1. A perturbation on $H_{\rm surf}$ in the regime $J \gg J'$, by, for example, a magnetic field, acts like a string tension that reduces the amplitude of large loops (on a vacuum reference state). In fact, there are two phases as a function of the strength of the perturbation. For very weak perturbations, it has been argued that the loop-order parameter scales with the perimeter of the loop, whereas for strong perturbations it scales with the area[46]. These are known as deconfined and confined phases in analogy to lattice gauge theory and are examples of phenomena that could be observed using our protocol. It may also be interesting to consider adapting the present protocol to spin–lattice systems with non-abelian anyons[47].

METHODS

SELECTIVE ADDRESSING

To achieve selective addressing with submicrometre resolution, a further strong control beam (different from the control beam for the ancilla spin) couples the atomic excited state $|e\rangle$ with the auxiliary metastable state $|r\rangle$, which is initially empty. The control beam is tuned to two-photon resonance with the cavity mode as indicated in Fig. 2b. Effectively, the strong control field switches off the interaction of all atoms with the cavity mode by driving them into the 'dark state'[26,27]. Only if the control field vanishes exactly at the position of the atom, will the atom interact with the cavity mode. The problem of selective addressing is thus reduced to the problem of creating the control beam with an intensity profile having nodes at desired positions. As detailed in the Supplementary Information, the latter can be achieved with a set of laguerre–gaussian modes created by holograms[48].

As discussed in ref. 27, addressing errors are associated with two effects: (1) each trapped atom has a finite spread around the lattice points, whereas the addressing beam vanishes only at the lattice points, and consequently there will always be a tiny but finite coupling between the addressing beam and selected spins; (2) the finite lifetime for the metastable state $|r\rangle$ will induce errors for unselected spins. For example, the estimated error probability associated with each addressing site can be $\varepsilon_{\rm address} \approx 0.01$ for ^{87}Rb trapped in a deep optical lattice[27]. In addition, for Kitaev's honeycomb-lattice model (Fig. 1b), the effective leakage error can be $\varepsilon_{\rm hcb} \approx 0.01$ for parameters $J_x/J_z = J_y/J_z = 0.2$ (ref. 33). For anyonic braiding operations addressing $L = 25$ sites, the overall fidelity $(1 - \varepsilon_{\rm address} - \varepsilon_{\rm hcb})^L \approx 0.60$ should provide sufficient contrast for anyonic interferometry.

The addressing error probability can be further suppressed by increasing trapping confinement, using laguerre–gaussian beams with larger winding number, applying shaped pulses with optimal control and choosing long-lived auxiliary state $|r\rangle$. This will enable us to carry out braiding operations with longer strings. Alternatively, we may adiabatically expand the entire lattice, carry out operations over selected sites and adiabatically restore the lattice to the initial spacing. The expansion/restoration of the lattice can be done without changing the trapping wavelength, by either changing the angle between the lattice beams[49] or using holographic techniques to create optical lattices[48]. The addressing errors can be negligibly small for the expanded lattice. The errors associated with the expansion/restoration are dominated by the sites farther away from the centre of the lattice, because they move faster than those sites close to the centre. To suppress such errors, we may freeze all interactions among the lattice sites (by increasing the lattice barriers before the expansion and restoring them after the restoration of the lattice) and carry out the expansion/restoration as slowly as possible.

DERIVATION OF THE GEOMETRIC PHASE GATE

We describe the necessary elements to construct the geometric phase gate shown in Fig. 3. First, we require the displacement operator $D(\xi) \equiv e^{\xi a^\dagger - \xi^* a}$ that can be obtained by injecting coherent states through cavity mirrors. The amplitude and phase of the injected field determine the phase-space displacement of the bosonic field by ξ.

Second, we need the displacement operation that depends on the state of the memory spins:

$$D(i\alpha S_C^Z) = \begin{cases} D(i\alpha) & \text{if } \langle S_C^z \rangle = +1 \\ D(-i\alpha) & \text{if } \langle S_C^z \rangle = -1, \end{cases}$$

where we use $\langle S_C^z \rangle = \pm 1$ to represent the ± 1 subspaces of the memory spins associated with the operator S_C^z. We can achieve $D(i\alpha S_C^Z)$ by applying the QND hamiltonian for time $t_C = \pi/2|\chi|$ with coupling χ before the displacement operation $D(\alpha e^{i\phi})$ followed by the QND interaction again for time t_C but with coupling $-\chi$. The justification is based on the identity

$$D(\alpha e^{i\phi + i\theta O}) = R(\theta O) D(\alpha e^{i\phi}) R(-\theta O),$$

with $R(x) = e^{ixa^\dagger a}$ and the two commuting operators $[O, a] = 0$. For $O = \sum_{j \in C} \sigma_j^z$ and $\theta = \pi/2$, we have $e^{i\phi + i\theta O} = e^{i\phi} \prod_{j \in C} e^{i\pi/2 \sigma_j^z} = e^{i(\phi + m\pi/2)} S_C^z$, with $m = N_C$. Conditioned on $\phi = -(m-1)\pi/2$, we obtain $D(\alpha e^{i\phi + i\theta O}) = D(i\alpha S_C^Z)$.

Third, we need dispersive coupling between the bosonic field and the ancilla spin (with two levels $\{|0\rangle_A, |1\rangle_A\}$)

$$V_A = \chi_A a^\dagger a |1\rangle_A\langle 1|,$$

with coupling strength χ_A, which can be switched on and off using optical control[26,27] or mechanical displacement of the ancilla spin. With such dispersive interaction, we are able to obtain the displacement operation conditioned on the state of the ancilla spin, $D(\beta|1\rangle_A\langle 1|) = |0\rangle_A\langle 0| \otimes \mathbf{I} + |1\rangle_A\langle 1| \otimes D(\beta)$, by the following procedure: (1) apply the interaction V_A for time $t_A = \pi/\chi_A$, (2) displace the bosonic field by $-\beta/2$, (3) apply the interaction V_A again for time t_A and (4) displace the bosonic field by $\beta/2$. Steps 1–3 displace the bosonic field by $\mp\beta/2$ for the ancilla spin in state $|0\rangle_A$ and $|1\rangle_A$, respectively. Combined with the displacement $\beta/2$ from step (4), we have the operation $D(\beta|1\rangle_A\langle 1|)$.

Finally, the controlled-string operation is a combination of the above elements:

$$U = D(-\beta|1\rangle_A\langle 1|_A) D(-i\alpha S_C^z) D(\beta|1\rangle_A\langle 1|_A) D(i\alpha S_C^z). \qquad (7)$$

The bosonic field is restored to its initial state, while accumulating a phase depending on both the state of the ancilla spin and the value for the string operator as shown in Fig. 3.

FRINGE CONTRAST OF THE INTERFEROMETER IN THE PRESENCE OF EXCITATIONS

We refer to anyons left from the initialization as quenched anyons, which can result in measurable effects to the phase measurement associated with braiding (equation (5)). To be specific, we will consider the planar code, and assume

© 2008 Nature Publishing Group

that the probability to have one pair of initial anyons is p while neglecting the case with multiple pairs of anyons. If the anyons are immobile (for example, the braiding operation is much faster than anyonic propagation), the contrast of the phase measurement depends only on the probability that the loop $l_1 \cup l_3$ (or $l'_2 \cup l'_4$) (Fig. 4a) encloses an odd number of initial x-particles (or z-particles). An extra phase $e^{i\theta} = -1$ will be accumulated from each loop satisfying this condition. Suppose the loop $l_1 \cup l_3$ (or $l'_2 \cup l'_4$) encloses m faces (or m' vertices). If one pair of initial x-particles is uniformly distributed among $N^2 \times (N^2-1)/2$ possible configurations, the probability for accumulating an extra phase is $q_m \equiv 2m(N^2-m)/(N^2(N^2-1))$ for the loop $l_1 \cup l_3$. The probability reaches a maximum value $\approx 1/2$ for $m \approx N^2/2$; meanwhile it vanishes for $m = 0$ or N^2, which is achieved by $l_1 = l_3$. Therefore, the contrast for the fringes of $\langle \sigma_\phi \rangle$ versus ϕ will be reduced to $1 - p \times (q_m + q_{m'})$.

If the anyons are highly diffusive (for example, random anyonic propagation is very fast compared with the intervals between the control operations), we should avoid adding any anyons by applying string operators that act within the ground subspace of the topological memory. As shown in Fig. 4c, we use generators of the encoded qubits associated with strings $\{l_{Z1}, l'_{X2}, l_{Z3}, l'_{X4}\}$ to implement the braiding operation. However, any quenched anyons (if present) will quickly diffuse over the entire torus and completely wash away the fringe of $\langle \sigma_\phi \rangle$. Therefore, the remaining contrast with highly diffusive anyons is $1-p$. Note that imperfect string operators may also reduce the contrast, because they may introduce unwanted anyons to the topological memory with probability approximately proportional to the length of the string.

EXTENSION TO $\mathbb{Z}_d$ GAUGE THEORIES

This interferometric technique can be extended to measure abelian anyonic statistics for any $\mathbb{Z}_d$ gauge theory by introducing the spin–lattice hamiltonian with d levels for each spin[50]. A probe qubit can still be used to measure the statistical phase via controlled-string operations. The mutual statistical phase between a charge $a \in \mathbb{Z}_d$ and flux $b \in \mathbb{Z}_d$ associated with the braiding operation is $\tilde{Z}^a_{\mathcal{C}'_Z} \tilde{X}^{-b}_{\mathcal{C}'_X} \tilde{Z}^a_{\mathcal{C}_Z} \tilde{X}^b_{\mathcal{C}_X} = e^{i2\pi ab/d}$. Here, the string operator $\tilde{Z}^a_{\mathcal{C}_Z}$ ($\tilde{X}^b_{\mathcal{C}_X}$) is a product of Z^a (X^b) operators of all the spins on the string $\mathcal{C}_Z$ ($\mathcal{C}_X$), where Z and X are elements of the generalized Pauli group. The operator Z can be implemented by phasing pairs of spin states at a time using the protocols in the main text for the appropriate duration at each stage. Equivalently, field polarizations and detunings can be chosen so that only one of the d levels is strongly coupled to the cavity, then evolve that state for the appropriate time, and swap other states in, evolve, and swap out again. A total of $d-1$ global gates suffice to simulate $\tilde{Z}^a_{\mathcal{C}_Z}$. The same follows for the $X^b_{\mathcal{C}_X}$ operators, but a parallel Fourier transform operator $F = \prod_{j \in \mathcal{C}_X} f_j$ must be carried out first on all of the spins in the configuration, before implementing $Z^b_{\mathcal{C}_X}$, then applying F^{-1}.

Received 9 November 2007; accepted 13 March 2008; published 20 April 2008.

References

1. Wen, X.-G. *Quantum Field Theory of Many-Body Systems: From the Origin of Sound to an Origin of Light and Electrons* (Oxford Univ. Press, Oxford, 2004).
2. Einarsson, T. Fractional statistics on a torus. *Phys. Rev. Lett.* **64**, 1995–1998 (1990).
3. Das Sarma, S., Freedman, M., Nayak, C., Simon, S. H. & Stern, A. Non-abelian anyons and topological quantum computation. Preprint at <http://arxiv:0707.1889> (2007).
4. Camino, F. E., Zhou, W. & Goldman, V. J. Realization of a Laughlin quasiparticle interferometer: Observation of fractional statistics. *Phys. Rev. B* **72**, 075342 (2005).
5. Rosenow, B. & Halperin, B. I. Influence of interactions on flux and back-gate period of quantum Hall interferometers. *Phys. Rev. Lett.* **98**, 106801 (2007).
6. Kitaev, A. Anyons in an exactly solved model and beyond. *Ann. Phys.* **321**, 2–111 (2006).
7. Duan, L. M., Demler, E. & Lukin, M. D. Controlling spin exchange interactions of ultracold atoms in optical lattices. *Phys. Rev. Lett.* **91**, 090402 (2003).
8. Micheli, A., Brennen, G. K. & Zoller, P. A toolbox for lattice-spin models with polar molecules. *Nature Phys.* **2**, 341–347 (2006).
9. Brennen, G. K. & Pachos, J. K. Why should anyone care about computing with anyons? *Proc. R. Soc. Lond. A* **464**, 1–24 (2007).
10. Pachos, J. K. The wavefunction of an anyon. *Ann. Phys.* **322**, 1254–1264 (2007).
11. Zhang, C. W., Scarola, V. W., Tewari, S. & Das Sarma, S. Anyonic braiding in optical lattices. *Proc. Natl Acad. Sci. USA* **104**, 18415–18420 (2007).
12. Mabuchi, H. & Doherty, A. C. Cavity quantum electrodynamics: Coherence in context. *Science* **298**, 1372–1377 (2002).
13. Gupta, S., Moore, K. L., Murch, K. W. & Stamper-Kurn, D. M. Cavity nonlinear optics at low photon numbers from collective atomic motion. *Phys. Rev. Lett.* **99**, 213601 (2007).
14. Colombe, Y. *et al.* Strong atom-field coupling for Bose–Einstein condensates in an optical cavity on a chip. *Nature* **450**, 272–276 (2007).
15. Brennecke, F. *et al.* Cavity QED with a Bose–Einstein condensate. *Nature* **450**, 268–271 (2007).
16. Cirac, J. I. & Zoller, P. Quantum computations with cold trapped ions. *Phys. Rev. Lett.* **74**, 4091–4094 (1995).
17. Lu, C.-Y., Gao, W.-B., Guhne, O., Zhou, X.-Q. & Chen, Z.-B. Demonstration of fractional statistics of anyons in the Kitaev lattice-spin model. Preprint at <http://arxiv:0710.0278> (2007).
18. Pachos, J. K. *et al.* Revealing anyonic statistics with multiphoton entanglement. Preprint at <http://arxiv:0710.0895> (2007).
19. Han, Y. J., Raussendorf, R. & Duan, L. M. Scheme for demonstration of fractional statistics of anyons in an exactly solvable model. *Phys. Rev. Lett.* **98**, 150404 (2007).
20. Briegel, H. J., Dur, W., Cirac, J. I. & Zoller, P. Quantum repeater: The role of imperfect local operations in quantum communication. *Phys. Rev. Lett.* **81**, 5932–5935 (1998).
21. Jiang, L., Taylor, J. M., Khaneja, N. & Lukin, M. D. Optimal approach to quantum communication algorithms using dynamics programming. *Proc. Natl Acad. Sci. USA* **104**, 17291–17296 (2007).
22. Kitaev, A. Y. Fault-tolerant quantum computation by anyons. *Ann. Phys.* **303**, 2–30 (2003).
23. Dennis, E., Kitaev, A., Landahl, A. & Preskill, J. Topological quantum memory. *J. Math. Phys.* **43**, 4452–4505 (2002).
24. Trotzky, S. *et al.* Time-resolved observation and control of superexchange interactions with ultracold atoms in optical lattices. *Science* **319**, 295–299 (2008).
25. Scully, M. O. & Zubairy, M. S. *Quantum Optics* (Cambridge Univ. Press, Cambridge, 1997).
26. Cho, J. Addressing individual atoms in optical lattices with standing-wave driving fields. *Phys. Rev. Lett.* **99**, 020502 (2007).
27. Gorshkov, A., Jiang, L., Greiner, M., Zoller, P. & Lukin, M. D. Coherent quantum optical control with sub-wavelength resolution. *Phys. Rev. Lett.* **100**, 093005 (2008).
28. Wang, X. & Zanardi, P. Simulation of many-body interactions by conditional geometric phases. *Phys. Rev. A* **65**, 032327 (2002).
29. Purcell, E. M. Spontaneous emission probabilities at radio frequencies. *Phys. Rev.* **69**, 681 (1946).
30. Michler, P. *et al.* A quantum dot single-photon turnstile device. *Science* **290**, 2282–2285 (2000).
31. Vandersypen, L. M. K. & Chuang, I. L. NMR techniques for quantum control and computation. *Rev. Mod. Phys.* **76**, 1037–1069 (2004).
32. Brown, K. R., Harrow, A. W. & Chuang, I. L. Arbitrarily accurate composite pulse sequences. *Phys. Rev. A* **70**, 052318 (2004).
33. Dusuel, S., Schmidt, K. P. & Vidal, J. Creation and manipulation of anyons in the Kitaev model. Preprint at <http://arxiv:0802.0379> (2008).
34. Duan, L. M., Blinov, B. B., Moehring, D. L. & Monroe, C. Scalable trapped ion quantum computation with a probabilistic ion-photon mapping. *Quant. Inf. Comput.* **4**, 165–173 (2004).
35. Lim, Y. L., Barrett, S. D., Beige, A., Kok, P. & Kwek, L. C. Repeat-until-success quantum computing using stationary and flying qubits. *Phys. Rev. A* **73**, 012304 (2006).
36. Benjamin, S. C., Browne, D. E., Fitzsimons, J. & Morton, J. J. L. Brokered graph-state quantum computation. *New J. Phys.* **8**, 141 (2006).
37. Jiang, L., Taylor, J. M., Sorensen, A. & Lukin, M. D. Distributed quantum computation based-on small quantum registers. *Phys. Rev. A* **76**, 062323 (2007).
38. Arovas, D., Schrieffer, J. R. & Wilczek, F. Fractional statistics and the quantum Hall effect. *Phys. Rev. Lett.* **53**, 722–723 (1984).
39. Freedman, M., Nayak, C. & Shtengel, K. Extended NMR model with ring exchange: A route to a non-abelian topological phase. *Phys. Rev. Lett.* **94**, 066401 (2005).
40. Doucot, B., Feigel'man, M. V., Ioffe, L. B. & Ioselevich, A. S. Protected qubits and Chern-Simons theories in Josephson junction arrays. *Phys. Rev. B* **71**, 024505 (2005).
41. Nielsen, M. A. & Chuang, I. *Quantum Computation and Quantum Information* (Cambridge Univ. Press, Cambridge, 2000).
42. Levitt, M. H. *Spin Dynamics: Basics of Nuclear Magnetic Resonance* (Wiley, Chichester, 2001).
43. Bacon, D. Operator quantum error-correcting subsystems for self-correcting quantum memories. *Phys. Rev. A* **73**, 012340 (2006).
44. Milman, P. *et al.* Topologically decoherence-protected qubits with trapped ions. *Phys. Rev. Lett.* **99**, 020503 (2007).
45. Levin, M. A. & Wen, X. G. String-net condensation: A physical mechanism for topological phases. *Phys. Rev. B* **71**, 045110 (2005).
46. Hastings, M. B. & Wen, X.-G. Quasiadiabatic continuation of quantum states: The stability of topological ground-state degeneracy and emergent gauge invariance. *Phys. Rev. B* **72**, 045141 (2005).
47. Aguado, M., Brennen, G. K., Verstraete, F. & Cirac, J. I. Creation, manipulation and detection of anyons in optical lattices. Preprint at <http://arxiv:0802.3163> (2008).
48. Grier, D. G. A revolution in optical manipulation. *Nature* **424**, 810–816 (2003).
49. Porto, J. V., Rolston, S., Tolra, B. L., Williams, C. J. & Phillips, W. D. Quantum information with neutral atoms as qubits. *Phil. Trans. R. Soc. Lond. A* **361**, 1417–1427 (2003).
50. Bullock, S. S. & Brennen, G. K. Qudit surface codes and gauge theory with finite cyclic groups. *J. Phys. A* **40**, 3481–3505 (2007).

Supplementary Information accompanies this paper on www.nature.com/naturephysics.

Acknowledgements

We gratefully acknowledge conversations with H. P. Buchler, S. Dusuel, M. Greiner, L. Ioffe, A. Peng, A. M. Rey and J. Vidal. Work at Harvard is supported by NSF, ARO-MURI, CUA, DARPA, AFOSR and the Packard Foundation. Work at Innsbruck is supported by the Austrian Science Foundation, the EU under grants OLAQUI, SCALA, and the Institute for Quantum Information.

Author information

Reprints and permission information is available online at http://npg.nature.com/reprintsandpermissions. Correspondence and requests for materials should be addressed to L.J.

© 2008 Nature Publishing Group